A discriminative feature selection approach for shape analysis: application to fetal brain cortical folding study

J Pontabry, François Rousseau, C Studholme, M Koob, J.-L Dietemann

A discriminative feature selection approach for shape analysis: application to fetal brain cortical folding study

J. Pontabry[a,*], F. Rousseau[b], C. Studholme[c], M. Koob[b,d], J.-L. Dietemann[b,d]

[a] *Institut de Génétique et de Biologie Moléculaire et Cellulaire, CNRS-INSERM-Université de Strasbourg, France*
[b] *Laboratoire ICube, CNRS-Université de Strasbourg, France*
[c] *Biomedical Image Computing Group, Departments of Pediatrics, Bioengineering and Radiology, University of Washington, Seattle, USA*
[d] *Service de Radiopédiatrie, Hôpital de Hautepierre, Strasbourg, France*

Abstract

The development of post-processing reconstruction techniques has opened new possibilities for the study of in utero fetal brain MRI data. Recent cortical surface analysis have led to the computation of quantitative maps characterizing brain folding of the developing brain. In this paper, we describe a novel feature selection-based approach that can be used for studying the most discriminative brain folding patterns using in utero reconstructed fetal MR data. Results show that this temporal process related to brain maturation can be characterized by a small set of points, located in the main sulci.

Keywords: Structural MRI, Fetal imaging, Feature selection, Brain development

1. Introduction

Development of the central nervous system (CNS) is governed by a complex set of several spatio-temporal mechanisms. Understanding this sequence is fundamental for understanding perinatal neurology (Volpe, 2008). Many processes are involved in brain development at fetal and neonatal stages. These are asynchronous processes taking place at different locations in the brain. For instance, the main period of neural migration is 5 to 25 week post-menstrual age (PMA). Once neurons have been generated, they migrate through two different mechanisms (passive cell displacement and active cell migration). Axon and dendrite sprouting starts around 25 weeks PMA and declines around 1 year. The brain is also the scene of other major events such as synapse formation, glial cell proliferation, myelination, etc. (see de Graaf-Peters and Hadders-Algra (2006) for a recent review of the ontogeny of the human CNS).

As highlighted by de Graaf-Peters and Hadders-Algra (2006), the knowledge on the exact timeline of ontogenetic events occurring during human brain development will provide new insights on the influence of injuries appearing at a specific point in time during this important period of brain building. The modeling of this process timeline from in vivo data is of great importance for improving, for instance, neonatal care services. It is clear that fetal and neonatal periods are key steps of brain development and a better understanding of the involved mechanisms is a corner stone in perinatal care.

Recent advances in ultrafast MRI sequences (such as half-Fourier turbo spin echo (HASTE) (Yamashita et al., 1997) or single shot fast spin echo (SSFSE) (Busse et al., 2000)) associated with the development of new techniques of image processing for retrospective motion correction (Rousseau et al., 2005) enabled to study *in vivo* fetal brain development. Since 2005, several two-step registration-based reconstruction techniques have been proposed to estimate a 3D high resolution image from sets of scattered T2-weighted slices (Jiang et al., 2007, Kim et al., 2010, Limperopoulos and Clouchoux, 2009, Rousseau et al., 2006). These reconstruction techniques have been further enhanced by including super-resolution framework (Gholipour et al., 2010, Kuklisova-Murgasova et al., 2012, Rousseau et al., 2010). Following these works on 3D fetal brain image reconstruction, several dedicated segmentation methods have been proposed (Caldairou et al., 2011, Dittrich et al., 2014, Gholipour et al., 2012, Habas et al., 2010b). See the work of Studholme (2011) for further reading on fetal MRI reconstruction and segmentation.

The development of these post-processing techniques had led to new ways to perform structural development studies of the fetal brain. Based on local volume changes using tensor-based morphometry techniques, maps of fetal brain growth patterns have been estimated leading to the detection of the emergence of sulci and gyri by differentiating between the changes in the cortical plate and the underlying cerebral mantle (Rajagopalan et al., 2011). This work has been extended to examine not only scalar expansion of tissue but the directional components of that

*Corresponding author
Email addresses: pontabry@unistra.fr (J. Pontabry), rousseau@unistra.fr (F. Rousseau)

expansion (Rajagopalan et al., 2012). The availability of high resolution 3D images of the fetal brain with tissue labelling enables also studies of tissue boundary shape changes. This has led to the computation of quantitative maps of brain folding further used for statistical detection of sulci and brain asymmetry emergence (Habas et al., 2012). Cortical folding analysis has been also used to predict physiological age (Wright et al., 2014). Such brain folding studies are of great importance to improve our understanding of malformation of the cortex.

In this work, we focus on the study of the evolution of brain folding during later stages of intrauterine life. Instead of computing scalar features such as surface curvature to provide global markers of brain development, we have chosen to investigate the use of a data driven approach. The underlying question is: what is the smallest most discriminative set of features reflecting fetal brain folding? Following the work of Rajagopalan et al. (2012), a deformation based morphometry approach is adopted to capture directional growth information on the white matter / cortex interface. However, the voxel-based statistical testing method applied in (Rajagopalan et al., 2012) does not lead to easily interpretable results of growth patterns. In this study, we have considered the use of feature selection techniques in order to extract the sparsest set of deformation fields describing the brain folding process. By studying brain development as a shape modeling problem, we are able to extract the most discriminative set of points related to brain folding during in utero development.

2. Materials and Methods

2.1. Subjects and fetal MRI acquisition

This study has been conducted on a population of 22 fetus aged from 26 to 34 weeks of gestational age at scan time. The data set includes 23 MRI T2 weighted images. Fetal MRI images have been obtained on a 1.5 T Siemens Avanto MRI Scanner (SIEMENS, Erlangen, Germany) using a 6-channel phased array coil combined to the spine array positioned around the mother abdomen. The resolution of the T2 weighted HASTE sequence (TE/TR = 147/3190 ms) is: $0.74 \times 0.74 \times 3.45$mm.

2.2. Image reconstruction and segmentation

Raw dataset has been preprocessed using the "Baby Brain Toolkit" (BTK) in order to increase image quality without modifying the acquisition protocol used in routine (Rousseau et al., 2013). The retrospective motion correction method is based on a registration refined compounding of multiple sets of orthogonal fast 2D MRI slices to address the problem of fetal motion. This is achieved by first globally registering the low resolution images, and then applying an iterative slice alignment scheme which seeks to refine the 3D positioning of each slice to the current combined high resolution volume. This is driven by normalized mutual information to provide robustness to contrast variation induced by motion of the fetal brain with respect to the imaging coil in the magnet. Moreover, a super-resolution technique is applied in order to remove the effects of the blurring convolution and to increase the voxel grid density. The resolution of the reconstructed images is: $0.74 \times 0.74 \times 0.74$mm. A topological based clustering technique is then applied on the motion-compensated high-resolution images to provide segmentation maps (ventricles, CSF, cortical plate, non-cortical plate -including white matter, subplate, intermediate zone and deep gray nuclei) (Caldairou et al., 2011).

2.3. Brain image normalization

Adopting a standard approach for deformation based morphometry to compare anatomies at different stages of brain development, a mapping is estimated to bring every subject's anatomy into correspondence within a common coordinate system. This common space corresponds to the average space of the subjects's anatomies. For this purpose, an iterative registration approach proposed by Guimond *et al.* (Guimond et al., 2000) has been used in this work. The procedure to estimate a common space is as following. First, a reference image is chosen among the dataset and the non linear transformations from this reference to the remaining images of the dataset are estimated using ANTS diffeomorphic registration technique (Avants and Gee, 2004). Then, the choice of a reference induces a bias that is corrected by using the average of all transformations. Finally, this average transformation maps the chosen reference to a new space which corresponds to the average space of the subject's anatomies. The reference for the next iteration will be this new space. These steps are repeated iteratively, until convergence of the algorithm, which usually occurs within a few iterations (Guimond et al., 2000).

Parameters for ANTS registration are: cross correlation as similarity measure, gaussian regularization with a symmetric diffeomorphic transformation model. To avoid any possibility of mis-registration due to brain tissue contrast changes, the similarity criterion used during the registration process is a weighted combination of image intensities and tissue label maps (a similar strategy has been proposed by Habas et al. (2010a)). Weights have been set to 0.5 for each feature.

To assess the quality of the atlas building step based on image registration, we have computed the average DICE coefficient of the white matter maps between the estimated template and the population. This average DICE coefficient is equal to 0.95 ± 0.06, showing the validity of the approach.

2.4. Feature selection

Our objective concerns the selection of the most discriminative deformation-based features reflecting fetal brain development. Please note that although we focus in this work on brain folding, the proposed approach is versatile

and it could be used with any other kind of relevant features dedicated to brain anatomy study.

Let be $\mathcal{P} = \{I_1, I_2, \ldots, I_N\}$ a set of N images. Theses images are normalized in an average space $\overline{I}$ computed as described previously in section 2.3. The transformation $\mathcal{T}_i$ that maps the average space $\overline{I}$ to the image I_i is a composition of an affine transform and a non-linear deformation field. In order to capture local shape changes, we only consider the non linear components of the mappings $\{\mathcal{T}_i\}_{i=1,\ldots,N}$.

Each of the N non linear deformation fields that maps voxels from average space to population space consists of M vectors of $\mathbb{R}^3$ (where M is the number of voxels considered in the region of interest). These 3D vectors are further arranged in a matrix $\boldsymbol{Y} \in \mathcal{M}_{M\times N}(\mathbb{R}^3)$ where the rows and columns correspond respectively to the features and the samples:

$$\boldsymbol{Y} = \begin{pmatrix} \vec{p}_{1,1} & \cdots & \vec{p}_{1,N} \\ \vdots & \ddots & \vdots \\ \vec{p}_{M,1} & \cdots & \vec{p}_{M,N} \end{pmatrix} \quad , \tag{1}$$

where $\vec{p}_{i,j}$ is the 3D displacement vector of the voxel i in the deformation field of subject j. Since we focus in this study on brain folding, the analysis is restricted to the displacement vectors belonging to the cortical plate. The matrix $\boldsymbol{Y}$ is the full set of features from which a sparse representation of brain folding is estimated. Instead of adopting a voxel-based approach, that is to say applying a statistical testing method to detect the most significant folding patterns, we propose a data driven approach aiming at extracting from the matrix $\boldsymbol{Y}$ a small set of discriminative features.

Such a dimension reduction issue can be tackled with either feature extraction or feature selection techniques. Feature extraction methods transform the high-dimensional data into a space of fewer dimensions. The main linear technique is the principal component analysis (PCA) which performs a linear mapping of the data to a lower-dimensional space in such a way that the variance in the low-dimensional representation is maximized and the covariance is minimized. Although PCA may be applied to study affine deformation, the linear assumption makes it less adapted for non linear deformations. Non-linear feature extraction techniques have been proposed by preserving local data structures. An important example of such non linear techniques is Isomap (Tenenbaum et al., 2000) (see Gerber et al. (2010) for an example of Isomap application to manifold modeling for MRI dataset analysis). However, the lower-dimensional space may not be easily interpretable, meaning that in our context, the extracted patterns do not correspond to displacement fields anymore. In this work, we investigate an alternate method by relying on a feature selection approach, aiming at computing a subset of the original variables.

Let Y_j be the j^{th} column of the matrix $\boldsymbol{Y}$ and X_j a subset vector of Y_j ($X_j \subset Y_j$) of size $M' \leq M$. The key assumption here is that the entire set of non linear deformations can be reconstructed using only a very small set of 3D displacement vectors. Within such a sparse framework, Y_j and X_j are linked by a reconstruction function f:

$$Y_j = f(X_j). \tag{2}$$

In this work, we chose to formulate the reconstruction function f using a Nadarya-Watson kernel regression function (Nadaraya, 1964):

$$\hat{f}(X, h) = \sum_{j=1}^{N} w_j(X, h) Y_j \tag{3}$$

where the weighting function w_j is written as

$$w_j(X, h) = \frac{K_h(X - X_j)}{\sum_{k=1}^{N} K_h(X - X_k)} \quad . \tag{4}$$

The parameter h is the bandwidth of the kernel K_h acting on the subset X. The proposed sparsity-based approach relies on the assumption of redundant information in the original sample Y. Therefore, the relevant information is carried by a subset of parameters. Such a subset of M' parameters should minimize the following criterion:

$$\{\hat{\gamma}, \hat{h}\} = \arg\min_{\gamma, h} J(\gamma, h) \text{ s.t. } \|\gamma\|_0 \leq M' \quad , \tag{5}$$

where $\gamma \in \mathcal{M}_{p\times 1}(\{0, 1\})$ is a binary vector used to define the activated parameters and J is the reconstruction error defined as follows:

$$J(\gamma, h) = \sum_{j=1}^{N} \left\| Y_j - \hat{f}(\text{diag}(\gamma) \cdot Y_j, h) \right\|_2 \quad . \tag{6}$$

Optimization problems such as defined by equation (5) are NP-hard problems because of the use of L0 norm (Elad, 2010). In this work, we used an alternate optimization scheme, i.e. the two parameters of interest $\{\gamma, h\}$ are estimated alternatively. The estimation of the bandwidth parameter h is performed using a gradient descent technique within a leave-one-out strategy (Wand and Jones, 1995). The estimation of the activation vector γ is obtained using a greedy algorithm (Pudil et al., 1994) with a complexity of $\mathcal{O}(pM')$ cost function evaluations. The vector γ is first initialized to the null vector. Then, M' features at most are added iteratively. At each step, the feature added is the feature that maximizes the decrease of the reconstruction error. This procedure is detailed in algorithm 1.

The following convergence criterion have been defined for the proposed algorithm:

1. the maximal number of parameter to select M' is reached;
2. no parameter can be added without increasing the cost function;

3. the reconstruction error is lower than a predefined error threshold $\mathcal{E}$.

The error criterion is the mean reconstruction error of parameters and is then expressed in mm:

$$\bar{\mathcal{E}}(\gamma, h) = \frac{1}{Np} \sum_{j=1}^{N} \sum_{i=1}^{p} \left\| Y_{i,i} - \hat{f}(\mathrm{diag}(\gamma) \cdot Y_j, h)_i \right\|_2 \quad , \quad (7)$$

where $\hat{f}(\mathrm{diag}(\gamma) \cdot Y_j, h)_i$ is the reconstruction of the i^{th} displacement vector of the j^{th} subject.

Algorithm 1: Feature selection algorithm

Input:
- $\boldsymbol{Y}$ Set of deformation fields
- P Maximum number of parameters to select
- $\mathcal{E}$ Error threshold

Output:
- $\boldsymbol{X}$ Selected features

$\gamma := (0 \cdots 0)^T$
Estimate parameter h
$J_0 := J(\gamma, \hat{h})$
$k := 1$

while $k \leq M'$ *and* $J(\gamma, \hat{h}) \leq \mathcal{E}$ **do**
  $J_k := J_{k-1}$
  foreach *feature* i *such that* $\gamma(i) = 0$ **do**
    $\gamma(i) := 1$
    if $J(\gamma, \hat{h}) < J_k$ **then**
      $J_k := J(\gamma, \hat{h})$
      $i_k^{(+)} := i$
    end
    $\gamma(i) := 0$
  end
  if *one parameter to add is found* **then**
    $\gamma\left(i_k^{(+)}\right) := 1$
    Estimate parameter h
    $k := k + 1$
  else
    Stop the loop
  end
end
$\boldsymbol{X} := \mathrm{diag}(\gamma) \cdot \boldsymbol{Y}$

3. Results

Experiments have been conducted on both synthetic and real datasets. In the first part, the behavior and the performance of the algorithm are studied on the synthetic dataset. Then, in a second part, the proposed method is applied on in vivo fetal brain dataset.

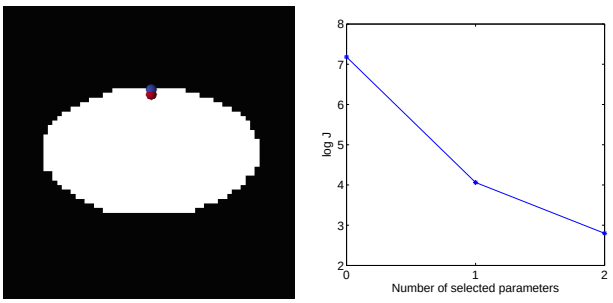

(a) Selected points (b) Cost function evolution

Figure 2: Selected points and cost function evolution of the proposed algorithm on a synthetic dataset. The colors reflect the energy of the parameters as a log scale. The first selected parameter (in red) is located on the border of the ellipse and on the varying axe of the dataset. The cost function decreases dramatically after one selected parameter and no parameter can be added without increasing the cost function after 2 iterations.

In each experiment, a Gaussian kernel is used within the reconstruction function (see equation (3)) and the maximum number of parameter is set to $M' = 100$. The mean parameter error threshold is set to $\mathcal{E} = 0.1$ mm for experiments on brain MR images. For synthetic experiment only, the threshold is set to $\mathcal{E} = 0$ mm in order to study the convergence of the algorithm.

3.1. Synthetic dataset experiments

The synthetic dataset is composed of 20 two-dimensional ellipses (rasterized to images of size 64×64 pixels) whose shape varies according to the vertical axis (see Figure 1). The first image of this dataset is then an elongated ellipse while the last image is a circle. This dataset has been generated using only one degree of freedom (i.e. the length of the vertical axis). On the first image, the vertical axis is four times smaller than the horizontal one.

The results of the proposed algorithm on synthetic dataset are depicted in Figure 2(a). Convergence is reached in this experiment when only 2 features have been selected. Indeed, adding more features do not make the cost function decrease. The evolution of the cost function is shown in Figure 2(b) and suggests that the first selected point captures the main variability of the dataset. Moreover, it has to be noticed that the two selected points are located on the vertical axis where the shape variability is high. Due to the symmetric experimental setup, only one selected point location should be necessary to describe the growth pattern. This is confirmed by looking at the residual reconstruction error shown in Figure 3. The residual errors (displayed in log scale) decrease dramatically after the selection of the first parameter and are mainly located on the borders of the vertical axis. Then, the decrease of residual errors after the selection of the second point is negligible.

The selected parameters are supposed to represent the variability of the shapes. The set of 20 shapes shown in figure 1 can be seen in two different ways: 1) as a set

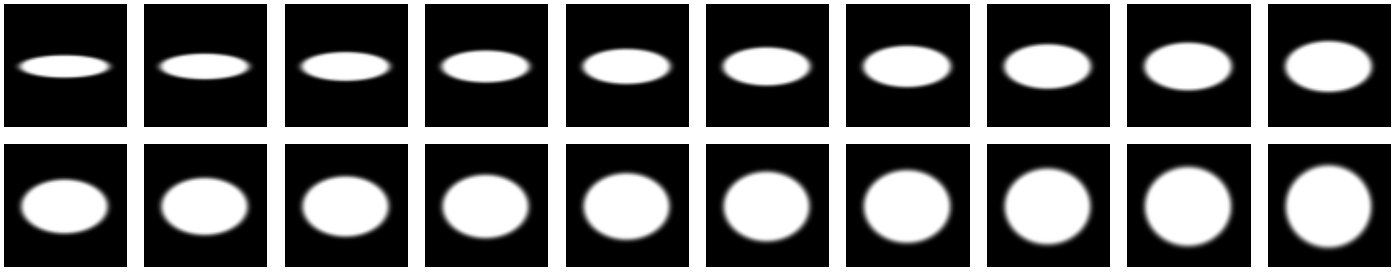

Figure 1: Dataset used in the synthetic experiment, composed of 20 images of size 64×64 pixels. The 2D shapes are varying according to the vertical axis.

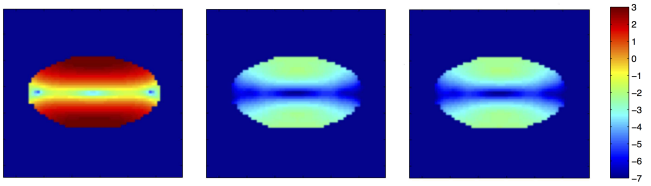

(a) $p' = 0$ (b) $p' = 1$ (c) $p' = 2$

Figure 3: Residuals visualization on the synthetic dataset for 0, 1 and 2 selected parameters (displayed with a log scale). After one selected parameter, the residuals decrease dramatically.

of 20 different shapes (reflecting shape variability), or 2) as a set of an evolving shape over time (i.e. temporal evolution of a shape). In later case, it is interesting to study time varying features that could reflect the growth rate for instance, such as length of the vertical axis.

Given the half-size d of the ellipse on the vertical axis and at $t = 1$, the half-size of the ellipse on the same axis and at $t = 20$ should be equal to $4d - d = 3d$, because the vertical axis on the first image is four time smaller than the same axis on the last image. Since there are 20 images sampled over time, the growth rate should be equal to $\frac{3d}{20} = 0.15d$. In our case, the half-size of the vertical axis on the first image is 5.5 pixels. Therefore, the theoretical growth rate of the simulated dataset is 0.825 pixels per time unit.

Figure 4 shows the mean magnitude of vectors over time in the reference space of the first image ($t = 1$). The linear function fitted to the data has a slope of 0.812, which is close to the theoretical growth rate.

3.2. Application on fetal brain MRI dataset

Since our first objective is to study the geometrical changes of the cortical folding through in utero brain maturation, we define as region of interest the cortical gray matter. Moreover, average deformation fields (computed in the orthogonal direction of brain surface) along the cortical gray matter have been used in order to reduce the initial parameter set to a smaller set of 3D displacement vectors (Rajagopalan et al., 2012). Figure 5 shows five examples of deformation fields considered in this study.

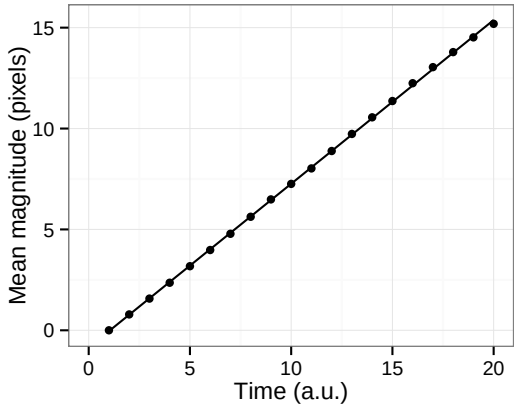

Figure 4: Analysis of the growth rate on the synthetical dataset. The plot shows the mean magnitude of selected vectors across time (in the reference space of the first image, $t = 1$). By studying the fit of a linear function, the growth rate can be estimated with the slope of the function. In this case, the estimated growth rate (0.812) is close the theoretical one (0.825).

3.2.1. Influence of the bandwidth parameter h

In this experiment, we evaluate the influence of the bandwidth parameter h over the selected points. Here, we applied the selection algorithm by setting manually this parameter $h \in \{0.5, 1, 1.5, 2, 3\}$. The results obtained applying the algorithm on the temporal lobe for different values for h are displayed in figure 6. First, it can be easily seen that increasing the value of h makes the number of selected points increase. Please note that h is a parameter that controls the smoothness of the non parametric regression and therefore the value of h is related to the sparsity of the solution. Second, this experiment also shows the location stability of the selected features. It appears that the selected points are located in the main sulci (superior temporal sulcus, inferior temporal sulcus, lateral sulcus) in this region of interest, appearing during the considered period of age. This is a key point since it means that modifications of the bandwidth only influence the number of selected points, not their locations (i.e. the estimated growth pattern). The value of the bandwidth h does not modify the spatial pattern of the most discriminative selected points. Third, the experiment, restricted on the temporal lobe area, shows that growth variability

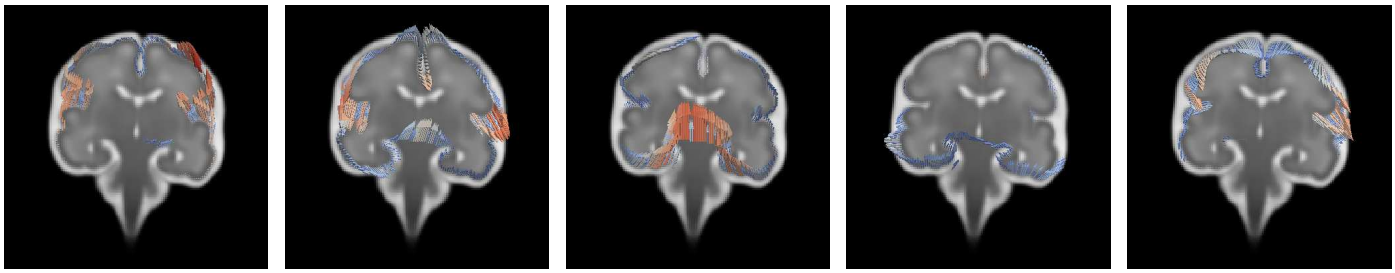

Figure 5: Five instances of the dataset used. The selection algorithm is applied on the cortical deformation fields mapping the reference space to population.

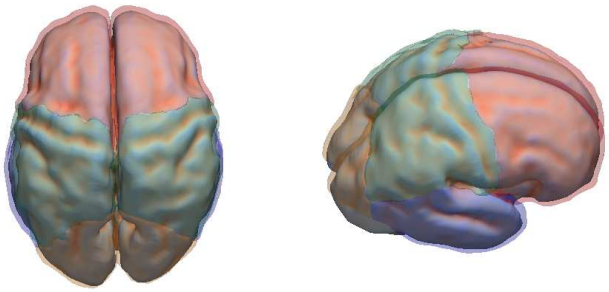

Figure 7: The regions of interest used with the feature selection algorithm. These regions corresponds approximately to the frontal (red), temporal (blue), parietal (green) and occipital (yellow) lobes.

can be captured by few points in the sulci of interest.

Please note that in the proposed algorithm, the bandwidth parameter h is estimated at each iteration using a leave-one-out strategy in order to minimize the variance of the regression function. For the next experiments, h is then computed automatically.

3.2.2. Points selection on fetal brain lobes

In this section, we propose to apply the feature selection algorithm onto 8 regions of interest (ROI) corresponding approximately to the frontal, temporal, parietal and occipital lobes of each hemisphere (see figure 7) in order to characterize spatial pattern of cortical folding for the considered period of age (26 to 34 weeks). Each of these ROI have been considered independently.

Experiments previously described have shown that the selected points tend to be in sulci valleys. Thus, the ROI defined here do not exactly match the anatomical lobes to avoid any bias of selected sulci. For instance, the central sulcus should define the boundary between the frontal and parietal lobes. However, we chose to associate the central sulcus with the parietal lobe, in order to give a chance to the algorithm to select cortical points of this sulcus.

The results of the selection algorithm on brain lobes are displayed in figures 8 and 9 respectively for lobes in left and right hemispheres. For each considered ROI, four types of results are provided : (a) selected points when the bandwidth h is set to 2, (b) selected points when h is automatically estimated, (c) a coronal view showing the location of selected points and (d) the evolution of the cost function. While the first visualization (using $h = 2$) provides the main patterns of selected features, the second visualization (using automatic bandwidth computation) shows the sparsity of the reached solution of the algorithm. Only few features (up to 6) are required to discriminate the sets of images for each ROI. The coronal view confirms previous experiments (see Section 3.2.1): the selected points are located into sulci valleys.

3.2.3. Evolution of deformation vector magnitude

We examine in this section the temporal evolution of magnitudes of selected deformation vectors. Once the most discriminant points are selected for each region of interest, we compute the set $\mathcal{V}$ of deformation fields between each subject and the mean image estimated at 26 weeks: $\mathcal{V} = \{\vec{v}_{\mathbf{x}}(t_i)\}$ where $\mathbf{x}$ is the location of each selected point and t_i is the time difference between the age of the subject i and 26 weeks. The evolution of the magnitudes of computed deformation fields at selected point locations is estimated using a temporal polynomial of degree 3 regression approach (see figure 10 for an instance of regression over time for one vector). Figure 11 shows (a) the time evolution of the mean magnitude for the eight considered ROI (corresponding to the left-right lobes), (b) the mean magnitude for the 4 ROI by fusing data from left and right hemispheres, and (c) the mean magnitude by considering only left vs right. It can be seen that mean magnitude at occipital lobe has a different temporal evolution from the three other anatomical regions. Moreover, temporal differences in left and right temporal evolution are also observed. Statistical testing on larger dataset has to be conducted in order to verify the significance of these observations.

3.3. Discussion

In this paper, we have shown that early cortical folding patterns occurring during fetal brain development can be expressed by a sparse representation using a feature selection approach. By using sparse non linear deformation fields, we have highlighted major cortical surface changes in the considered age interval. Such information extraction is important since sulci can be used to discriminate brain development stages. The period of age considered

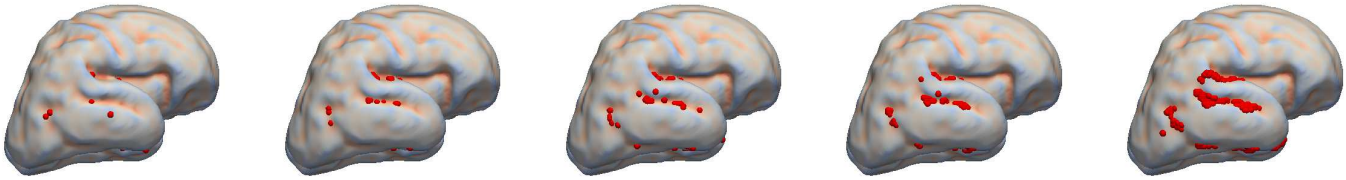

(a) $h = 0.5$ (b) $h = 1$ (c) $h = 1.5$ (d) $h = 2$ (e) $h = 3$

Figure 6: Study of the influence of the choice of the bandwidth parameter of the proposed algorithm. As the bandwidth increases, the number of selected parameters increases as well. An important property is the location stability of the solution with various bandwidth values.

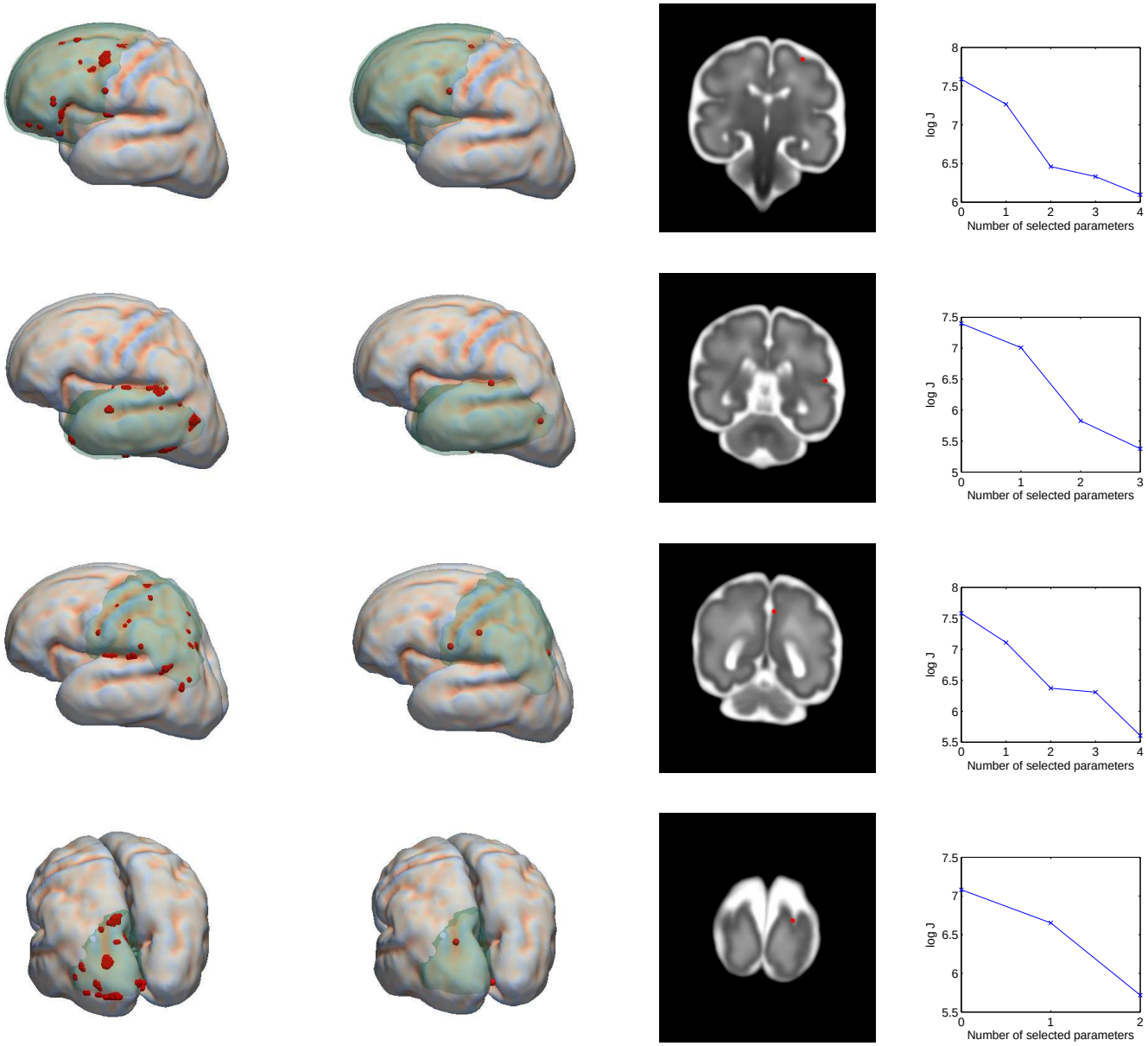

(a) $h = 2$ (b) Optimal h (c) Coronal plane (d) Cost functions

Figure 8: Selected cortical points on four lobe regions of the left hemisphere using the proposed algorithm. The left column shows the solution for a fixed bandwidth ($h = 2$). The other columns show the results for the optimal bandwidth. Top row: frontal lobe; second row: temporal lobe; third row: parietal lobe; last row: occipital lobe. The selected cortical points are depicted as red spheres. The color code in 3D mesh views maps the curvature of the cortical plate from blue color (positive curvature) to red color (negative curvature).

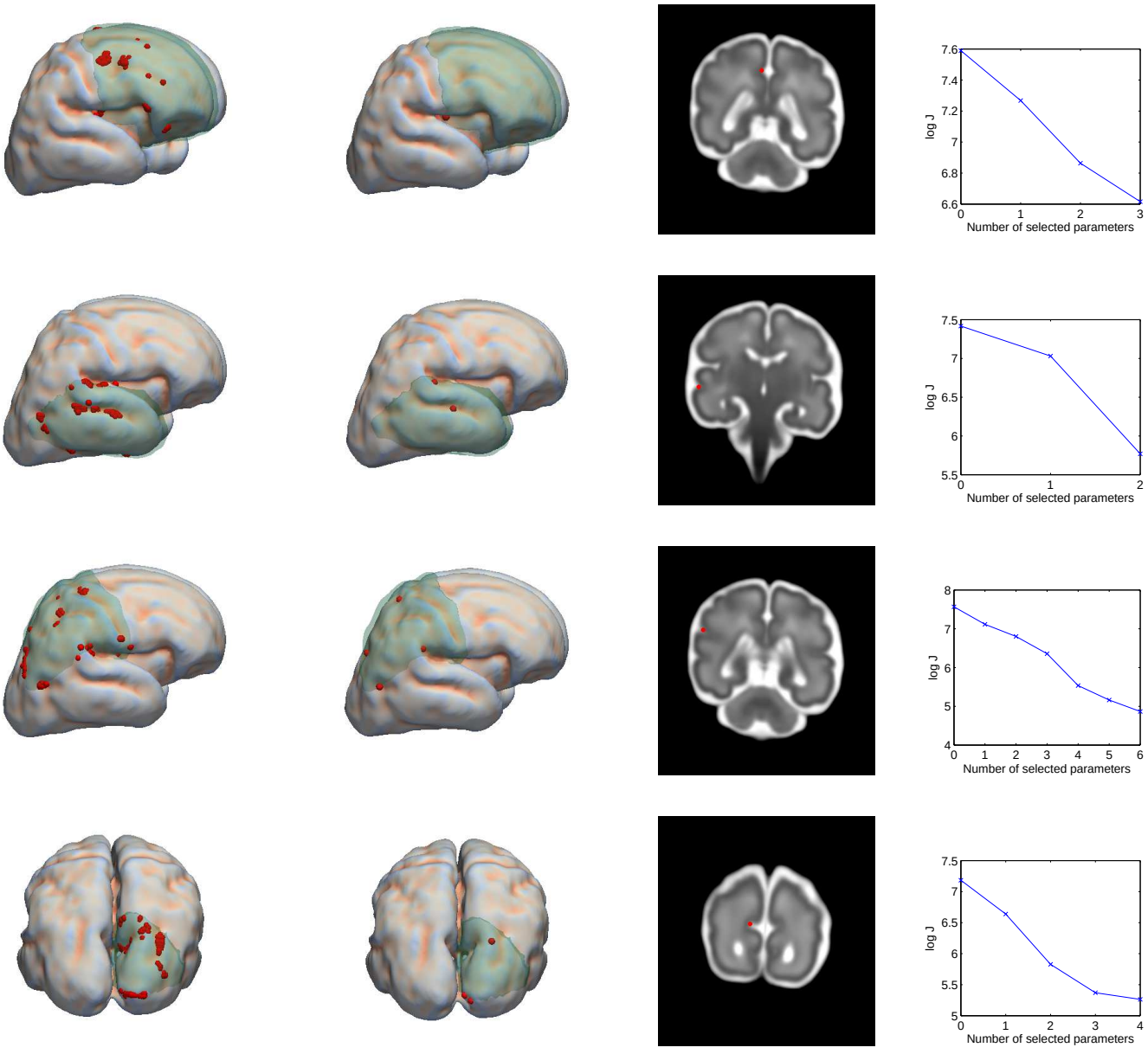

(a) $h = 2$ (b) Optimal h (c) Coronal plane (d) Cost functions

Figure 9: Selected cortical points of four lobe regions of the right hemisphere using the proposed algorithm. The left column shows the solution for a fixed bandwidth ($h = 2$). The other columns show the results for the optimal bandwidth. Top row: frontal lobe; second row: temporal lobe; third row: parietal lobe; last row: occipital lobe. The selected cortical points are depicted as red spheres. The color code in 3D mesh views maps the curvature of the cortical plate from blue color (positive curvature) to red color (negative curvature).

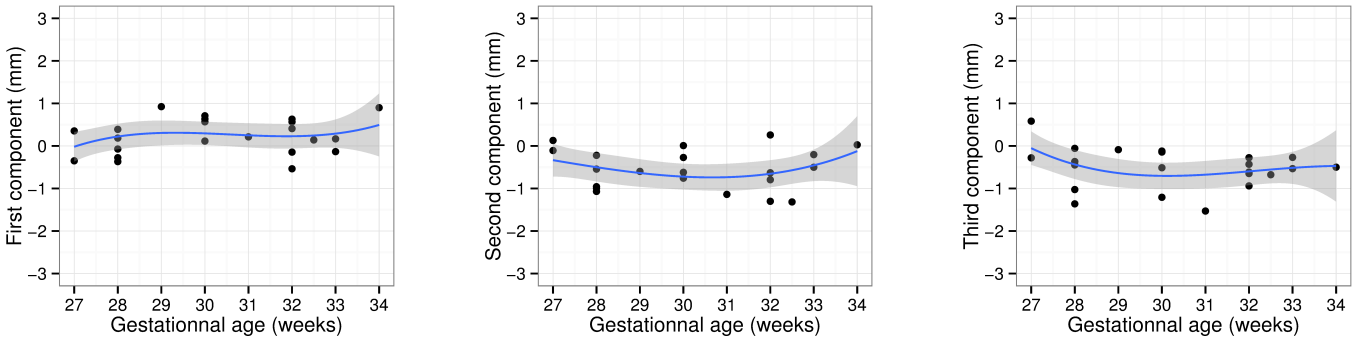

(a) First component (right to left)

(b) Second component (anterior to posterior)

(c) Third component (inferior to superior)

Figure 10: Example of polynomial regression over time (degree 3) for one selected vector of the right temporal lobe.

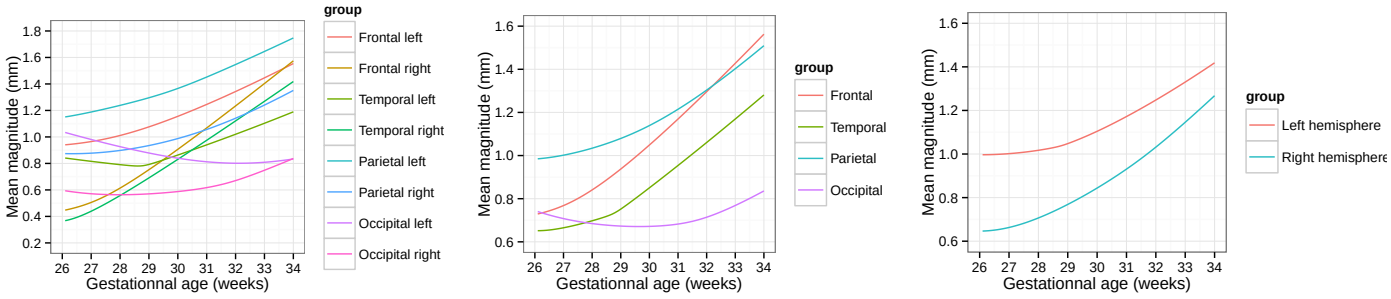

(a) All lobes

(b) 4 lobes

(c) Hemispheres

Figure 11: Mean magnitude of selected deformation vectors of lobes over time.

in this work (26 to 34 weeks) corresponds to a linear evolution of the surface curvature observed by Wright et al. (2014). Our experiments performed on mean magnitudes of deformation vectors tend to show the same trend.

In this work, we have considered non linear deformation fields providing voxel correspondence between each subject. Feature selection technique has been applied on these dense deformation fields in order to compute the smallest discriminative set of features characterizing the cortical folding process during fetal brain development. In this study, the registration step and the feature selection are independent. An alternative approach could have been to develop a registration technique incorporating a sparsity prior on the deformation fields. This kind of generative approach is related to the work of Durrleman *et al.* (Durrleman et al., 2012) in which a new parametrization of deformations is proposed in order to capture the variability in image ensembles. The key idea in their work is to select the most relevant control points and to estimate their positions in a template domain. A major difference between these two works is that control points may not belong to the shape under study. Thus, measuring the variability through the distribution of control points may not be easily interpretable with respect to the studied temporal process. By separating the registration step and the shape variability study, we can focus on shape deformation locally related to cortical folding.

Our work is also related to the recent study of growth seeds performed by Lefèvre et al. (2009), where an analysis of depth maps of cortical surface based on the Helmholtz decomposition of the deformation fields. In the work of Lefèvre et al. (2009), which is also related to the works of Cuzol et al. (2005) and Grenander et al. (2007), the main idea relies in that a decomposition is used to make the physical interpretation of the deformation fields (capturing the brain maturation process) easier. Our approach is complementary to these techniques in the sense that the relevant (i.e. most discriminative) displacement vectors are selected using a non-parametric approach. Further work would consist in analyzing the impact of the deformation model on the selected features.

As shown in our experiments, the most discriminative points lie in deep sulcal regions. These specific locations could be used as consistent shape features in further studies. Future work will consist in analyzing these patterns with regard to previous related works on sulcal root (Régis et al., 2005) and sulcal pit (Lohmann et al., 2008). It has been shown that deepest parts of sulci generally show less interindividual variability than superficial parts (Lohmann et al., 2008). The study of local fluctuations of these cortical patterns using a clustering approach such as in (Sun et al., 2009) could provide complementary insights on brain folding to gyrification index measurements (Clouchoux et al., 2011). The spatial distribution of deep sulcal landmarks (Im et al., 2010), especially over time (Meng et al., 2014), may help to set up new early markers of later functional development (Dubois et al., 2008) or particular cortical malformation (such as polymicrogyria) that might be difficult to detect and quantify visually.

4. Conclusion

In this paper, we have used a feature selection approach to characterize cortical folding patterns occurring during fetal brain development with a sparse representation.

The use of such a feature selection technique is not restricted to only fetal brain development studies. It could be used to define biomarkers, shape representation, diffusion / fiber tracts, etc.

Acknowledgment: The research leading to these results has received funding from the European Research Council under the European Community's Seventh Framework Programme (FP7/2007-2013 Grant Agreement no. 207667). This work is also funded by NIH Grant R01 NS055064.

References

Avants, B., Gee, J., 2004. Geodesic estimation for large deformation anatomical shape averaging and interpolation. NeuroImage 23, supplment 1, 139–150.

Busse, R. F., Riederer, S. J., Fletcher, J. G., Bharucha, A. E., Brandt, K. R., Sep. 2000. Interactive fast spin-echo imaging. Magnetic Resonance in Medicine 44 (3), 339–348.

Caldairou, B., Passat, N., Habas, P. A., Studholme, C., Koob, M., Dietemann, J.-L., Rousseau, F., 2011. Segmentation of the cortex in fetal MRI using a topological model. In: Biomedical Imaging: From Nano to Macro, 2011 IEEE International Symposium on. pp. 2045–2048.

Clouchoux, C., Kudelski, D., Gholipour, A., Warfield, S. K., Viseur, S., Bouyssi-Kobar, M., Mari, J.-L., Evans, A. C., du Plessis, A. J., Limperopoulos, C., May 2011. Quantitative in vivo MRI measurement of cortical development in the fetus. Brain Structure and Function 217 (1), 127–139.

Cuzol, A., Hellier, P., Mémin, E., 2005. A novel parametric method for non-rigid image registration. Information processing in medical imaging : proceedings of the ... conference 19, 456–467.

de Graaf-Peters, V. B., Hadders-Algra, M., Apr. 2006. Ontogeny of the human central nervous system: What is happening when? Early Human Development 82 (4), 257–266.

Dittrich, E., Riklin Raviv, T., Kasprian, G., Donner, R., Brugger, P. C., Prayer, D., Langs, G., Jan. 2014. A spatio-temporal latent atlas for semi-supervised learning of fetal brain segmentations and morphological age estimation. Medical Image Analysis 18 (1), 9–21.

Dubois, J., Benders, M., Borradori-Tolsa, C., Cachia, A., Lazeyras, F., Ha-Vinh Leuchter, R., Sizonenko, S. V., Warfield, S. K., Mangin, J. F., Hüppi, P. S., Jan. 2008. Primary cortical folding in the human newborn: an early marker of later functional development. Brain 131 (8), 2028–2041.

Durrleman, S., Allassonnière, S., Joshi, S., Aug. 2012. Sparse Adaptive Parameterization of Variability in Image Ensembles. International Journal of Computer Vision () 101 (1), 161–183.

Elad, M., 2010. Sparse and redundant representations: from theory to applications in signal and image processing. Springer.

Gerber, S., Tasdizen, T., Fletcher, P., Joshi, S., Whitaker, R., 2010. Manifold modeling for brain population analysis. Medical Image Analysis 14 (5), 64–653.

Gholipour, A., Akhondi-Asl, A., Estroff, J. A., Warfield, S. K., Apr. 2012. Multi-atlas multi-shape segmentation of fetal brain MRI for volumetric and morphometric analysis of ventriculomegaly. NeuroImage 60 (3), 1819–1831.

Gholipour, A., Estroff, J. A., Warfield, S. K., Oct. 2010. Robust super-resolution volume reconstruction from slice acquisitions: application to fetal brain MRI. IEEE Transactions on Medical Imaging 29 (10), 1739–1758.

Grenander, U., Srivastava, A., Saini, S., May 2007. A Pattern-Theoretic Characterization of Biological Growth. IEEE Transactions on Medical Imaging 26 (5), 648–659.

Guimond, A., Meunier, J., Thirion, J.-P., 2000. Average brain models: A convergence study. Computer Vision and Image Understanding 77 (2), 192–210.

Habas, P., Kim, K., Corbett-Detig, J., Rousseau, F., Glenn, O., Barkovich, A., Studholme, C., 2010a. A spatiotemporal atlas of mr intensity, tissue probability and shape of the fetal brain with application to segmentation. NeuroImage 53 (2), 460–470.

Habas, P. A., Kim, K., Rousseau, F., Glenn, O. A., Barkovich, A. J., Studholme, C., Aug. 2010b. Atlas-based segmentation of developing tissues in the human brain with quantitative validation in young fetuses. Human Brain Mapping 31 (9), 1348–1358.

Habas, P. A., Scott, J. A., Roosta, A., Rajagopalan, V., Kim, K., Rousseau, F., Barkovich, A. J., Glenn, O. A., Studholme, C., Jan. 2012. Early Folding Patterns and Asymmetries of the Normal Human Brain Detected from in Utero MRI. Cerebral Cortex 22 (1), 13–25.

Im, K., Jo, H. J., Mangin, J. F., Evans, A. C., Kim, S. I., Lee, J. M., Feb. 2010. Spatial Distribution of Deep Sulcal Landmarks and Hemispherical Asymmetry on the Cortical Surface. Cerebral Cortex 20 (3), 602–611.

Jiang, S., Xue, H., Glover, A., Rutherford, M., Rueckert, D., Hajnal, J. V., Jul. 2007. MRI of moving subjects using multislice snapshot images with volume reconstruction (SVR): application to fetal, neonatal, and adult brain studies. IEEE Transactions on Medical Imaging 26 (7), 967–980.

Kim, K., Habas, P. A., Rousseau, F., Glenn, O. A., Barkovich, A. J., Studholme, C., Jan. 2010. Intersection Based Motion Correction of Multislice MRI for 3-D in Utero Fetal Brain Image Formation. IEEE Transactions on Medical Imaging 29 (1), 146–158.

Kuklisova-Murgasova, M., Quaghebeur, G., Rutherford, M. A., Hajnal, J. V., Schnabel, J. A., 2012. Reconstruction of fetal brain MRI with intensity matching and complete outlier removal. Medical Image Analysis 16 (8), 1550–1564.

Lefèvre, J., Leroy, F., Khan, S., Dubois, J., Hüppi, P. S., Baillet, S., Mangin, J.-F., 2009. Identification of growth seeds in the neonate brain through surfacic Helmholtz decomposition. Information processing in medical imaging : proceedings of the ... conference 21, 252–263.

Limperopoulos, C., Clouchoux, C., Aug. 2009. Advancing fetal brain MRI: targets for the future. Seminars in perinatology 33 (4), 289–298.

Lohmann, G., von Cramon, D. Y., Colchester, A. C. F., May 2008. Deep Sulcal Landmarks Provide an Organizing Framework for Human Cortical Folding. Cerebral Cortex 18 (6), 1415–1420.

Meng, Y., Li, G., Lin, W., Gilmore, J. H., Shen, D., Oct. 2014. Spatial distribution and longitudinal development of deep cortical sulcal landmarks in infants. NeuroImage 100 (C), 206–218.

Nadaraya, E., 1964. On estimating regression. Theory of Probability and its Application 10, 186–190.

Pudil, P., Novovicova, J., Kittler, J., 1994. Floating search methods in feature selection. Pattern Recognition Letters 15 (11), 1119–1125.

Rajagopalan, V., Scott, J., Habas, P., Kim, K., Rousseau, F., Glenn, O., B., A., Studholme, C., 2012. Mapping directionality specific volume changes using tensor based morphometry: An application to the study of gyrogenesis and lateralization of the human fetal brain. NeuroImage 63 (2), 947–958.

Rajagopalan, V., Scott, J. A., Habas, P. A., Kim, K., Corbett-Detig, J. M., Rousseau, F., Barkovich, A. J., Glenn, O. A., Studholme, C., Feb. 2011. Local Tissue Growth Patterns Underlying Normal Fetal Human Brain Gyrification Quantified In Utero. Journal of Neuroscience 31 (8), 2878–2887.

Régis, J., Mangin, J.-F., Ochiai, T., Frouin, V., Riviére, D., Cachia, A., Tamura, M., Samson, Y., 2005. "Sulcal root" generic model: a hypothesis to overcome the variability of the human cortex folding patterns. Neurologia medico-chirurgica 45 (1), 1–17.

Rousseau, F., Glenn, O. A., Iordanova, B., Rodriguez-Carranza, C., Vigneron, D., Barkovich, A. J., Studholme, C., 2005. A novel approach to high resolution fetal brain MR imaging. International Conference on Medical Image Computing and Computer-Assisted Intervention: MICCAI 8 (Pt 1), 548–555.

Rousseau, F., Glenn, O. A., Iordanova, B., Rodriguez-Carranza, C., Vigneron, D. B., Barkovich, A. J., Studholme, C., Sep. 2006. Registration-Based Approach for Reconstruction of High-Resolution In Utero Fetal MR Brain Images. Academic Radiology 13 (9), 1072–1081.

Rousseau, F., Kim, K., Studholme, C., Koob, M., Dietemann, J.-L., 2010. On super-resolution for fetal brain MRI. International Conference on Medical Image Computing and Computer-Assisted Intervention: MICCAI 13 (Pt 2), 355–362.

Rousseau, F., Oubel, E., Pontabry, J., Schweitzer, M., Studholme, C., Koob, M., Dietemann, J.-L., 2013. Btk: An open-source toolkit for fetal brain mr image processing. Computer Methods and Programs in Biomedicine 109 (1), 65–73.

Studholme, C., Aug. 2011. Mapping Fetal Brain Development In Utero Using Magnetic Resonance Imaging: The Big Bang of Brain Mapping. Annual Review of Biomedical Engineering 13 (1), 345–368.

Sun, Z. Y., Perrot, M., Tucholka, A., Riviére, D., Mangin, J.-F., 2009. Constructing a dictionary of human brain folding patterns. International Conference on Medical Image Computing and Computer-Assisted Intervention: MICCAI 12 (Pt 2), 117–124.

Tenenbaum, J., de Silva, V., Langford, J., 2000. A global geometric framework for nonlinear dimensionality reduction. Science 290 (5500), 2319–2323.

Volpe, J. J., 2008. Neurology of the Newborn. Elsevier Health Sciences.

Wand, M., Jones, M., 1995. Kernel Smoothing. No. 60 in Chapman & Hall CRC Monographs on Statistics & Applied Probability. Chapman & Hall.

Wright, R., Kyriakopoulou, V., Ledig, C., Rutherford, M. A., Hajnal, J. V., Rueckert, D., Aljabar, P., May 2014. Automatic quantification of normal cortical folding patterns from fetal brain MRI. NeuroImage 91, 21–32.

Yamashita, Y., Namimoto, T., Abe, Y., Takahashi, M., Iwamasa, J., Miyazaki, K., Okamura, H., Feb. 1997. MR imaging of the fetus by a HASTE sequence. American Journal of Roentgenology 168 (2), 513–519.